

Review of the Multi-Input Single-Inductor Multi-Output (MISIMO) Energy Harvesting Interface Applied in Wearable Electronics

Zhuo Gao¹, Shiwei Wang², Yongfu Li¹ and Mingyi Chen^{1,*}

¹*Bio-Circuits and Systems Laboratory, Department of Micro-Nano Electronics, Shanghai Jiao Tong University, Shanghai, China*

²*Centre for Electronics Frontiers, School of Electronics and Computer Science, University of Southampton, Southampton, UK*

Correspondence*:
Mingyi Chen
mychen@sjtu.edu.cn

2 ABSTRACT

3 Along with the industrialization and popularization of the wearable electronics, an increasing
4 number of the wireless sensor nodes (WSNs) are deployed. Nevertheless, the conventional
5 battery-based power supply system has no longer satisfied the requirement of large-scale WSNs
6 in terms of battery life, which emerges the energy harvesting (EH) technique. In order to combine
7 various of energy sources and drive multi-loads, the multi-input single-inductor multi-output
8 (MISIMO) EH interface applied to wearable electronics is spotlighted. In this mini-review article,
9 the solutions for improving power conversion efficiency (PCE) and output quality in MISIMO
10 EH interface are summarized. Furthermore, the future trends of MISIMO EH interface are also
11 presented.

12 **Keywords:** wearable electronics, wireless sensor nodes, energy harvesting, MISIMO, power conversion efficiency, output quality

1 INTRODUCTION

13 Benefiting from the rapid development of the sensor technologies and the miniaturization of the electronics,
14 the wearable and implantable electronic devices have been widely used in biomedical research Yang et al.
15 (2019) Juteau and Gosselin (2020), motion detection Le et al. (2019) Dabbaghian et al. (2019) and health
16 monitoring Ding et al. (2021) Lee et al. (2020b). In such scenarios, the wireless sensor nodes (WSNs) are
17 in charge of monitoring the physical parameters and transmitting the digitized data. It is highly demanded
18 to prolong the usage time of the WSNs while subjecting to small-volume batteries. The typical power
19 consumption of a WSN is ranging from micro-watts (in idle state) to milli-watts (in active state), which
20 makes it feasible to be powered from the energy harvesting (EH) technique. The harvested energy is a
21 beneficial complement to battery energy, or more promising in the future, capable of fully taking the
22 place of the battery and leading to an energy autonomous WSNs. Fig. 1 shows such an autonomous WSN
23 supplied by the energy harvesting interface. The ambient energy sources can be extracted with the energy
24 transducer such as thermoelectric generators (TEG) Chen et al. (2019b) Coustans et al. (2019), photovoltaic
25 (PV) cells Jeong et al. (2020) Shim et al. (2019), triboelectric nanogenerators (TENG) Kara et al. (2021)
26 Niu et al. (2015), biofuel (BF) cells Talkhooncheh et al. (2021) Katic et al. (2018), **piezoelectric harvesters**

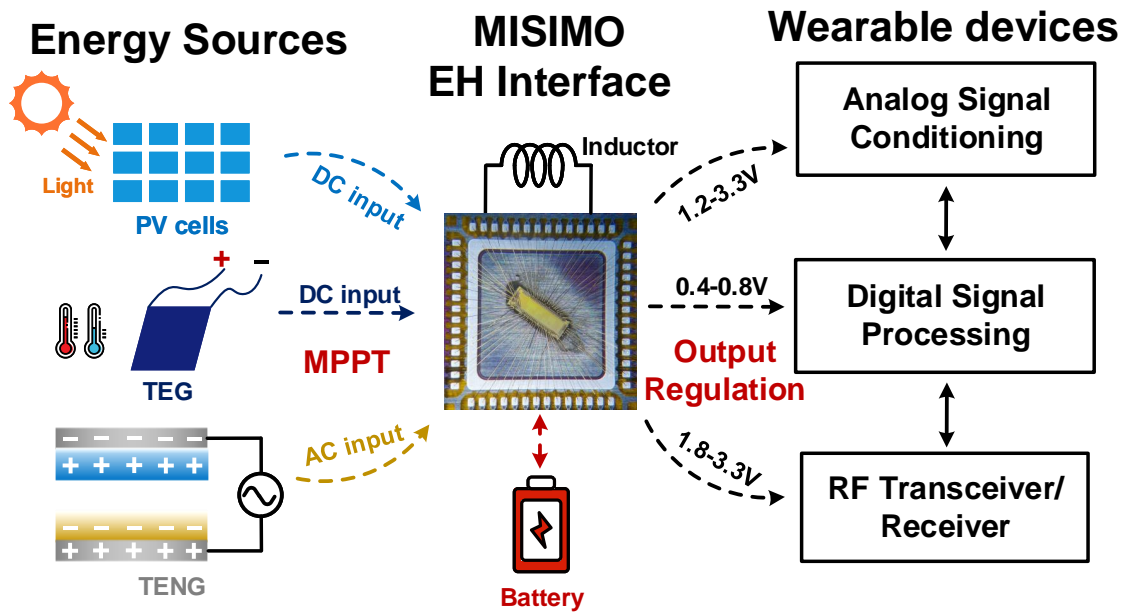


Figure 1. The MISIMO EH interface in the applications of WSN.

27 (PEH) Chen et al. (2020) Angelov and Nielsen-Lönn (2020) and RF energy harvester (RFEH) Martins
 28 and Serdijn (2021) Zeng et al. (2020), etc. However, the energy available from a single energy source is
 29 normally weak and stochastic, which is severely dominated by the changing environmental conditions. To
 30 combine various of energy sources, the multi-input with single-inductor solution is employed to increase
 31 the extracted power density while decreasing the volume of the bulky off-chip components. Moreover,
 32 considering the different load requirements of the analog signal conditioning, digital signal processing and
 33 RF transceiver/receiver blocks, multi-voltage domains are normally required to optimize the performance
 34 of each block independently. As a result, a multi-input single-inductor multi-output (MISIMO) energy
 35 harvesting interface applied to autonomous WSNs is of the most value and attracts lots of attentions.

36 However, the MISIMO EH interface faces two main problems. The first one is how to improve the
 37 power conversion efficiency (PCE). On the one hand, in the energy-constrained environment, a higher
 38 PCE ensures the sufficient power delivering to the loads. On the other hand, the MISIMO EH interface is
 39 generally designed to multi-modes for accommodating the various kinds of input and output conditions.
 40 It is challenging to optimize the power loss (including conduction, switching and control loss, etc) in
 41 different modes. Moreover, the energy transducer inherently has a changeable source resistance, thus the
 42 available power to the load can be maximized only if the equivalent input resistance of the converter equals
 43 to the source resistance according to the power delivery theory. Therefore, a simultaneous maximum power
 44 point tracking (MPPT) technique for each source has to be adopted for improving the end-to-end efficiency.
 45 The other problem is how to improve the output quality, including reducing the output voltage ripple and
 46 improving the load transient response. Due to the interaction between multi-output when the load condition
 47 is changing, the output voltage ripple is introduced. Large voltage ripple in digital circuit leads to high
 48 power consumption whereas it impacts the precision of the analog signal conditioning if the circuit is
 49 suffered from insufficient power supply rejection ratio (PSRR). To reduce the average power consumption,
 50 the WSN normally works in the heavily duty-cycle mode. The load current transits from the idle state to
 51 the active state from time to time. Thus the EH interface is highly demanded to have a rapid load transient

52 response within a wide load range. In the MISIMO EH interface with a battery as a supplement device for
53 energy delivery or storage, the interface can be easily kick-started. Nevertheless, the start-up circuit such as
54 a charge-pump Chen et al. (2019c) is indispensable if the stored component is a super capacitor.

55 In this mini-review paper, the state-of-the art solutions to solve these two problems are reviewed and
56 summarized, with the purpose to skeleton the future development of the relating research areas. The paper
57 is organized as follows: Section II summarizes the state-of-the-art techniques proposed in MISIMO EH
58 interfaces for improving the PCE and output quality. Section III draws the conclusion and presents the
59 future developing trends.

2 TECHNIQUES IN MISIMO ENERGY HARVESTING INTERFACE

60 In this section, the state-of-the-art techniques for improving the PCE and the output quality in MISIMO
61 EH interfaces for wearable electronics are reviewed.

62 2.1 Techniques for improving the PCE

63 Firstly, reducing power loss of the MISIMO EH interface is the straightforward method for the efficiency
64 optimization, which could be categorized as the reduction of the conduction loss, switching loss and the
65 control loss. The conduction loss mainly ascribes to the IR drop of the current flowing path, including the
66 power transistors, the off-chip inductor and the stored components. As a part from the aforementioned
67 conduction loss, MISIMO EH interfaces deliver the extra energy from the source to battery in light load
68 condition and supplement the insufficient energy from battery to load. As a result, the ‘double-conversion’
69 loss is introduced. The double-conversion rejection technique (DCRT) Kim et al. (2021) lowered the
70 trigger conditions of the source transferring the energy to the load directly, which avoids the excessive
71 participation of the battery, therefore the double-conversion loss can be reduced. Wang et al. (2020)
72 proposed the clockless shortest power path (CSPP) technique, which compares the output voltages and
73 the input voltages with their respective relaxation ranges of the reference voltages, then selects the right
74 input and output to achieve a shortest power path. In addition, turn-on resistance as well as the sizes of
75 the power transistors need to be optimized adaptively to match the various switching modes in MISIMO
76 EH interface. A reconfigurable and extendable Single-Inductor Single-Path three-switch (1P3S) converter
77 has been proposed in Huang and Kuo (2020), which can be reconfigurable or combined to the 2P3S or
78 2P6S converter according to various input voltages and output voltages, thus the appropriate power switch
79 sizes can be constituted for the suitable applications. Similarly, the 2P3S converter proposed in Wang
80 et al. (2016) is able to eliminate inductor-sharing power switches in a DISIDO converter, thus the reduced
81 conduction loss is achieved under the condition if the stored battery is initially charged and the most portion
82 of the load energy comes from the source. The switch size modulation (SSM) technique is adopted in
83 Amin and Mercier (2018), Kim et al. (2021), Qian et al. (2017). It applied modulated power switch sizes
84 and gate drivers according to various input source energy or load conditions since the inductor current
85 changes in different modes. The switching loss is mainly caused by the parasitic capacitance of the power
86 transistors which are charged before on-period and discharged before off-period. Since the switching
87 loss is proportional to the parasitic capacitance and the switching frequency, modulating the switching
88 frequency to accommodate the different modes is regarded as an effective method to reduce the switching
89 loss. Kuai et al. (2019) proposed the dual-frequency to accommodate different switching modes, where
90 the lower frequency clock CLK_L is employed in harvesting mode and the higher frequency clock CLK_H
91 is implemented in recycling mode. In the recycling mode, the battery supplements energy to the load
92 to complement the insufficient harvested energy, thus a smoothly high efficiency is maintained over a

93 wide dynamic range. The reversely polarized energy recycling (RPER) technique proposed in Chen et al.
94 (2019c) achieves a negative voltage stored in the output capacitor, thus a lower frequency is realized, at
95 the cost of slightly increasing of the conduction loss. Katic et al. (2018) sets four different frequencies
96 (1, 2, 4, and 8 kHz) for different input voltages, which provides the trade-off between the performance
97 and complexity. The control loss mainly comes from the quiescent power consumption of the analog
98 circuits such as bandgap references/comparators and dynamic power consumption of the digital logic
99 control circuits. Reducing the bias current is an efficient method to decrease the control loss in analog
100 circuits Gao et al. (2021). Substituting the analog circuits with digital circuits is getting trendy in many
101 low-power design Paidimarri and Chandrakasan (2017). As one known, the dynamic loss caused by the
102 digital circuits is proportional to the square of the supply voltage. **It is necessary to lower the supply**
103 **voltage of the control logic since its power consumption constitutes a large portion of the control loss**
104 **compared to the conventional EH interfaces. Therefore, the multi-voltage domain design technique is**
105 **generally employed to decrease the control loss.** When interface the low voltage control signal with the high
106 voltage power devices, level-shifters and gate drivers are normally needed Wang et al. (2020) Chen et al.
107 (2019c) Katic et al. (2018). The event-driven control techniques proposed in Wang et al. (2020) Kim et al.
108 (2018) Amin and Mercier (2018) feature of clock-less operation. The converter is triggered by the event
109 signal without a system clock. Therefore, both the quiescent and dynamic power loss are reduced. This
110 technique is beneficial particularly in the light load condition since the event-driven pulse frequency can be
111 significantly reduced compared to the conventional clock-driven converters. Moreover, the conduction loss
112 and switching loss are also decreased because of less conduction times of the power transistors.

113 Secondly, improving the MPPT efficiency is a crucial approach to improve the end-to-end efficiency
114 **and maximize the extracted energy. In the MISIMO EH interface that needs to combine the different**
115 **source energy, it is necessary to achieve the MPPT for each source simultaneously.** The fractional open
116 circuit voltage (FOCV) method has been widely used in MPPT owing to its low power consumption
117 and simplicity Chowdary et al. (2016). It samples the open circuit voltage (OCV) of the energy harvester,
118 subsequently the sampled voltage with a division ratio is compared with the input voltage of the converter.
119 The division ratio for each energy source is set to 0.625 (PV), 0.6 (BFC), and 0.5 (TEG) experimentally in
120 Kim et al. (2021), leading to poor adaptation. **The OCV is normally sampled from each source periodically**
121 **for the purpose of decreasing power consumption overhead. If multiple sources are prepared but only one**
122 **is selected, a relatively large input voltage ripple and a deviation from the MPP voltage could be introduced**
123 **from the not-chosen sources. The innovative dual-source mode proposed in Liu et al. (2018) extracts the**
124 **TEG and PV in one switching period, therefore, the input voltage ripple is reduced with a better tracking**
125 **efficiency. Ashraf (2020) introduced a short period before the inductor energizing phase to compare the**
126 **available input power of two TEG sources and decide which source is to be selected, the multiplexer block**
127 **changes the clock frequency for ensuring the systems always work at MPP.** Maeng et al. (2021) proposed a
128 calibration method through external register bits to control the division ratio, a higher tracking efficiency
129 can be achieved. **Hill climbing method is the other technique to achieve MPPT in MISIMO converters**
130 **which features of high tracking efficiency at the cost of a relatively complicated logic. It adjusts the on-time**
131 **of the power transistors to change the equivalent input resistances to different inputs.** The programmable
132 capacitor array (PCA) MPPT controller proposed in Qian et al. (2017) employs a high resolution 8-bit
133 capacitor array to adjust the on-time, so that the equivalent input resistance can be adjusted adaptively
134 with a peak tracking efficiency of 99.55%. Huang et al. (2018) proposed a periodic power integrator (PPI)
135 circuit. The input current proportional to the source power is integrated, so that the output level of PPI is
136 increased in case of sufficient source energy. The duty cycle generator with regarding to the output level
137 is then added to extend the on-time, a 99.2% tracking accuracy is achieved. Similarly, the internal power

138 monitor and tracking loop is proposed to automatically adjust the on-time to set the impedance of the
139 power converter to a desired value Bandyopadhyay and Chandrakasan (2012).

140 Thirdly, better switching control schemes lead to further increasing of PCE. When applied to EH for light
141 load wearable electronics, the MISIMO interfaces typically operates in the discontinuous conduction mode
142 (DCM), **which allows changing the input harvester without disrupting the operation of the converter.** In
143 DCM, the inductor is energized from zero current and deenergized to zero current without the need of
144 complex compensation techniques. Constant on-time (COT) or adaptive on-time (AOT) control methods
145 are widely adopted in DCM operation. **However, the converter cannot obtain the maximum PCE when**
146 **the input voltage varies with the COT control Chen et al. (2019c).** Liu et al. (2018) implemented the AOT
147 scheme with adaptive peak-inductor-current (APIC) to obtain high conversion efficiency under different
148 input voltages. To reduce the contention loss, the switch needs to be turned off when the current is zero.
149 It should be noteworthy that if the power transistors are not turned off in time, the reverse current may
150 be introduced in inductor deenergizing phase (off-time) that adversely affects the PCE. Thus to ensure
151 the exact zero current turning off point is indispensable in DCM. Normally, a comparator is utilized to
152 adjudge the zero current crossing point by comparing the inductor nodes with the reference (supply voltage
153 or ground). **As the change of the input or output voltage in each switching cycle leads to a variational**
154 **off-time, the static comparator is normally employed in the analog-based zero-current detector (ZCD)**
155 **to detect the zero current crossing point continuously. Nevertheless, the static comparator represents a**
156 **trade-off between comparison delay and power consumption.** To solve the above problem and eliminate
157 reverse current, Chen et al. (2019c) employed analog-based ZCD controller consisting of two common-gate
158 comparators with mismatched input pair transistors. The deliberate offset compensates the propagation
159 delay of the comparators in two directions. Similarly, Jung et al. (2020) employed an offset detector to
160 detect the positive or negative offset voltage of the comparator, then calibrate the offset adaptively. The
161 ZCD proposed in Kuai et al. (2019) eases the comparator design as it only has to slice two significantly
162 different voltages and compensate the delay by slicing in advantage of the zero-crossing point. The SSM
163 technique deployed in Amin and Mercier (2018) scaled down the size of the power transistors at light
164 load conditions, increasing the turn-on resistance, thus a node voltage with sufficiently high value can be
165 detected by the low-power comparator. Moreover, the comparators with offset added operate in duty-cycled
166 mode to reduce the power consumption. **The digital-based ZCD consisting of the dynamic comparator**
167 **features of none quiescent current consumption and high bandwidth. However, the rate of the off-time**
168 **calibration is related to the operation frequency of the dynamic comparator.** A delay-locked loop (DLL) is
169 utilized in Chen et al. (2019a) to accelerate the calibration. Lee et al. (2020a) implemented the constant
170 peak-inductor-current (CPIC) approach to fix the off-time under the same output voltage, where the on-time
171 is adaptively changed with different input voltage to satisfy the voltage-second balance. Therefore the
172 operation duration for the off-time calibration can be minimized thereby reducing the power consumption.

173 **2.2 Techniques for improving the output quality**

174 The MISIMO energy harvesting interface applied in WSNs is in charge of delivering the high quality
175 output to power the loads which features of the reduced output voltage ripple and the fast load transient
176 response with a wide load range. On the one hand, the relatively large voltage ripple will reduce the
177 noise immunity of digital circuit and impacts the accuracy in analog signal conditioning. **The output**
178 **voltage ripple is mainly caused by the insufficient energy delivering to the loads. In such scenario, the**
179 **outputs interact each other when a transition introduced by a certain load.** In order to reduce the output
180 voltage ripple, a large off-chip capacitor could be selected, however the volume and cost overhead will
181 be introduced. Charging each load in single cycle is an effective method to suppress the output voltage

Table 1. Comparison between state-of-the-art MISIMO EH interfaces.

	Process	Input sources	# of outputs	Techniques	Pros	Cons
Kim et al. (2021)	180 nm	PV,BF,TEG (3)	3	Double-Conversion Rejection	Reduced conduction loss	Large output voltage ripple
Lee et al. (2020a)	180 nm	PV,Battery (2)	2	2-D AOT (constant&adaptive)	Reduced on-time calibration & Reduced output voltage ripple	Reduced MPPT efficiency
Jung et al. (2020)	180 nm	DC voltage (4)	2	Optimal on-Time	Enhanced ZCD & Reduced output voltage ripple	Complicated control mechanism
Wang et al. (2020)	180 nm	PV,Battery (2)	3	Clockless Shortest Power Path	Reduced conduction & control loss	Reduced MPPT efficiency
Huang and Kuo (2020)	0.5 um	PV (2)	2	Reconfigurable and Extendable 1P3S	Reduced conduction loss	Hard to integrate
Chen et al. (2019c)	180 nm	PV,TEG (3)	2	Reversely Polarized Energy Recycling	Reduced switching loss	Increased conduction loss
Kim et al. (2018)	180 nm	PZ,PV (6)	9	Event-Driven	Enhanced load transient response	Increased switching loss
Huang et al. (2018)	180 nm	PV,TEG,BF (4)	4	PI-P&O MPPT	Reduced conduction loss & Increased MPPT efficiency	Reduced MPPT efficiency & load transient response
Liu et al. (2018)	180 nm	PV,TEG (2)	2	Dual-Source Mode	Increased MPPT efficiency & maximum available power	Reduced input sources
Amin and Mercier (2018)	28 nm	PV,BF,TEG (3)	3	Switch Size Modulation & Event-Driven control	Reduced conduction & control loss	Reduced PCE in heavy load
Qian et al. (2017)	350 nm	TEG,Battery (2)	2	Programmable-Capacitor -Array MPPT	Increased MPPT efficiency	Reduced PCE in light load

182 ripple. The inductor charging time under battery power calibration technique was proposed in Amin and
183 Mercier (2018), where the on-time for inductor energized from battery is calibrated with a load current
184 indicator, so that each load receives sufficient energy from the battery in a single cycle, reducing the output
185 voltage ripple. Qian et al. (2017) proposed the control mechanism of charging the dual output in single
186 inductor deenergizing phase, which greatly suppressed the output voltage ripple under light load condition.
187 Homoplastically, The buck-based dual-control mode proposed in Kim et al. (2021) charges the first output
188 in inductor energizing phase and the second output in deenergizing phase, which also powers the two
189 outputs in a single period resulting a reduced output voltage ripple. Other methods like 2-D AOT with
190 APIC technique implemented in Lee et al. (2020a) keeps a fixed ratio of ripple and output voltage values
191 when the output voltage is changing, so as to reduce the output voltage ripple. Nagateja et al. (2019)
192 employed a H-bridge capacitor to combine the AC and DC source energy before subsequently pumping it
193 up, which ensures a continuous inductor current that reduces output voltage ripple by 67%. On the other
194 hand, fast load transient response with a wide load range is also crucial for MISIMO converter since the
195 each output can vary from micro-watts to milli-watts when switching to the active state. Therefore, Qian
196 et al. (2018) proposed the charge sharing control technique, which adds a switch between the stored super
197 capacitor and the load. When the output voltage drops below the threshold voltage in the heavy load mode,
198 the charge stored in the super capacitor is shared through the direct path, achieving a smaller settling time
199 which leads to fast load transient response. Kim et al. (2018) deployed the event-driven control method, the
200 operated switching frequency can be raised to 25 MHz triggered by the event signal. The high-bandwidth
201 design optimally improve the load transient response. The clock skipping algorithm was proposed in Jung
202 et al. (2020), which optimally controls the number of clock skipplings according to the load condition. An
203 increasing the number of clocks occurrences under the condition from light load to heavy load, resulting in
204 a fast transient response for load regulation.

3 CONCLUSION

205 This mini-review article summarizes the techniques in MISIMO EH interface applied in the wearable
206 electronics. In terms of improving the PCE, several methods to reduce the power loss consisting of
207 the conduction loss, switching loss and control loss are introduced. Furthermore, improving the MPPT
208 efficiency and accuracy of ZCD are also the effective approach to improve the PCE. In terms of improving
209 the output quality, several techniques to suppress the output voltage ripple and achieve fast load transient
210 response are presented. **The pros and cons of the representative techniques employed in MISIMO EH**
211 **interfaces are organized in Table 1.**

212 The future trends of MISIMO EH interface are miniaturization by shrinking the size or avoiding the
213 usage of the off-chip components. It is because along with the industrialization and popularization of
214 the wearable electronics, an increasing number of the WSNs would be deployed, the relatively large
215 off-chip components is no longer matched with the smart sensor nodes. One possible solution proposed in
216 battery-based SIMO buck converter Chen and Fayed (2015) is raising the operation frequency, thus all the
217 passive components including the inductor and capacitors could be integrated on-chip, eventually leading to
218 a compact system solution. In addition, the techniques to reduce cross-regulation needs further investigation.
219 Since the multi-input have different electrical characteristics whereas the multi-outputs typically have
220 different load requirements, how to suppress their interaction is still a challenge for MISIMO EH interface.
221 Cross-regulation suppression is relatively well-addressed in battery-based SIMO buck converter while
222 still immature in MISIMO EH interface. In conclusion, it is foreseeable that with the development of
223 the aforementioned techniques, the fully on-chip autonomous WSNs will be generalized in wearable
224 electronics.

CONFLICT OF INTEREST STATEMENT

225 The authors declare that the research was conducted in the absence of any commercial or financial
226 relationships that could be construed as a potential conflict of interest.

AUTHOR CONTRIBUTIONS

227 The Author Contributions section is mandatory for all articles, including articles by sole authors. If an
228 appropriate statement is not provided on submission, a standard one will be inserted during the production
229 process. The Author Contributions statement must describe the contributions of individual authors referred
230 to by their initials and, in doing so, all authors agree to be accountable for the content of the work. Please
231 see here for full authorship criteria.

FUNDING

232 This research is supported in part by the National Key Research and Development Program of China under
233 Grant No. 2019YFB2204500; and in part by the Shanghai Pujiang Talent under Grant No. 20PJ1408600.

REFERENCES

234 Amin, S. S. and Mercier, P. P. (2018). Misimo: A multi-input single-inductor multi-output energy harvesting
235 platform in 28-nm fdsoi for powering net-zero-energy systems. *IEEE Journal of Solid-State Circuits* 53,
236 3407–3419. doi:10.1109/JSSC.2018.2865467

- 237 Angelov, P. and Nielsen-Lönn, M. (2020). A fully integrated multilevel synchronized-switch-harvesting-
238 on-capacitors interface for generic pehs. *IEEE Journal of Solid-State Circuits* 55, 2118–2128. doi:10.
239 1109/JSSC.2020.2979178
- 240 Ashraf, M. (2020). A maximum power-point tracking multiple-input thermal energy harvesting module.
241 *AEU - International Journal of Electronics and Communications* 121, 153231. doi:https://doi.org/10.
242 1016/j.aeue.2020.153231
- 243 Bandyopadhyay, S. and Chandrakasan, A. P. (2012). Platform architecture for solar, thermal, and vibration
244 energy combining with mppt and single inductor. *IEEE Journal of Solid-State Circuits* 47, 2199–2215.
245 doi:10.1109/JSSC.2012.2197239
- 246 Chen, C.-W. and Fayed, A. (2015). A low-power dual-frequency simo buck converter topology with
247 fully-integrated outputs and fast dynamic operation in 45 nm cmos. *IEEE Journal of Solid-State Circuits*
248 50, 2161–2173. doi:10.1109/JSSC.2015.2422782
- 249 Chen, I.-C., Liang, C.-W., and Tsai, T.-H. (2019a). A single-inductor dual-input dual-output dc–dc
250 converter for photovoltaic and piezoelectric energy harvesting systems. *IEEE Transactions on Circuits*
251 *and Systems II: Express Briefs* 66, 1763–1767. doi:10.1109/TCSII.2019.2921349
- 252 Chen, M., Yu, H., Wang, G., and Lian, Y. (2019b). A batteryless single-inductor boost converter with 190
253 mv self-startup voltage for thermal energy harvesting over a wide temperature range. *IEEE Transactions*
254 *on Circuits and Systems II: Express Briefs* 66, 889–893. doi:10.1109/TCSII.2018.2869328
- 255 Chen, P.-H., Cheng, H.-C., and Lo, C.-L. (2019c). A single-inductor triple-source quad-mode energy-
256 harvesting interface with automatic source selection and reversely polarized energy recycling. *IEEE*
257 *Journal of Solid-State Circuits* 54, 2671–2679. doi:10.1109/JSSC.2019.2917549
- 258 Chen, Z., Law, M.-K., Mak, P.-I., Zeng, X., and Martins, R. P. (2020). Piezoelectric energy-harvesting
259 interface using split-phase flipping-capacitor rectifier with capacitor reuse for input power adaptation.
260 *IEEE Journal of Solid-State Circuits* 55, 2106–2117. doi:10.1109/JSSC.2020.2989873
- 261 Chowdary, G., Singh, A., and Chatterjee, S. (2016). An 18 na, 87% efficient solar, vibration and rf
262 energy-harvesting power management system with a single shared inductor. *IEEE Journal of Solid-State*
263 *Circuits* 51, 2501–2513. doi:10.1109/JSSC.2016.2585304
- 264 Coustans, M., Krummenacher, F., and Kayal, M. (2019). A fully integrated 60 mv cold-start circuit for
265 single coil dc–dc boost converter for thermoelectric energy harvesting. *IEEE Transactions on Circuits*
266 *and Systems II: Express Briefs* 66, 1668–1672. doi:10.1109/TCSII.2019.2922683
- 267 Dabbaghian, A., Yousefi, T., Fatmi, S. Z., Shafia, P., and Kassiri, H. (2019). A 9.2-g fully-flexible
268 wireless ambulatory eeg monitoring and diagnostics headband with analog motion artifact detection and
269 compensation. *IEEE Transactions on Biomedical Circuits and Systems* 13, 1141–1151. doi:10.1109/
270 TBCAS.2019.2936327
- 271 Ding, X., Clifton, D., Ji, N., Lovell, N. H., Bonato, P., Chen, W., et al. (2021). Wearable sensing
272 and telehealth technology with potential applications in the coronavirus pandemic. *IEEE Reviews in*
273 *Biomedical Engineering* 14, 48–70. doi:10.1109/RBME.2020.2992838
- 274 Gao, Z., Chen, M., Liu, K., Zhao, J., Li, Y., and Wang, G. (2021). An asynchronous ac-dc boost converter
275 with event-driven voltage regulator and 94harvesting. *IEEE Transactions on Circuits and Systems II:*
276 *Express Briefs* 68, 2563–2567. doi:10.1109/TCSII.2021.3055949
- 277 Huang, C.-J., Ma, Y.-S., Yang, W.-H., Lin, Y.-T., Kuo, C.-C., Chen, K.-H., et al. (2018). A 99.2%
278 tracking accuracy single-inductor quadruple-input-quadruple-output buck-boost converter topology
279 with periodical interval perturbation and observation mppt. In *2018 IEEE Asian Solid-State Circuits*
280 *Conference (A-SSCC)*. 171–174. doi:10.1109/ASSCC.2018.8579308

- 281 Huang, P.-C. and Kuo, T.-H. (2020). A reconfigurable and extendable single-inductor single-path three-
282 switch converter for indoor photovoltaic energy harvesting. *IEEE Journal of Solid-State Circuits* 55,
283 1998–2008. doi:10.1109/JSSC.2020.2987722
- 284 Jeong, J., Shim, M., Maeng, J., Park, I., and Kim, C. (2020). An efficiency-aware cooperative multicharger
285 system for photovoltaic energy harvesting achieving 14 *IEEE Transactions on Power Electronics* 35,
286 2253–2256. doi:10.1109/TPEL.2019.2939170
- 287 Jung, J.-H., Jung, Y.-H., Hong, S.-K., and Kwon, O.-K. (2020). A high peak output power and high
288 power conversion efficiency simimo converter using optimal on-time control and hybrid zero current
289 switching for energy harvesting systems in iot applications. *IEEE Transactions on Power Electronics* 35,
290 8261–8275. doi:10.1109/TPEL.2019.2963513
- 291 Juteau, N. and Gosselin, B. (2020). Wearable wireless-enabled oscillometric sphygmomanometer: A
292 flexible ambulatory tool for blood pressure estimation. *IEEE Transactions on Biomedical Circuits and*
293 *Systems* 14, 1287–1298. doi:10.1109/TBCAS.2020.3026992
- 294 Kara, I., Becermis, M., Kamar, M. A.-A., Aktan, M., Dogan, H., and Mutlu, S. (2021). A 70-to-2
295 v triboelectric energy harvesting system utilizing parallel-sshi rectifier and dc-dc converters. *IEEE*
296 *Transactions on Circuits and Systems I: Regular Papers* 68, 210–223. doi:10.1109/TCSI.2020.3025468
- 297 Katic, J., Rodriguez, S., and Rusu, A. (2018). A high-efficiency energy harvesting interface for implanted
298 biofuel cell and thermal harvesters. *IEEE Transactions on Power Electronics* 33, 4125–4134. doi:10.
299 1109/TPEL.2017.2712668
- 300 Kim, H., Maeng, J., Park, I., Jeon, J., Lim, D., and Kim, C. (2021). A 90.2% peak efficiency multi-input
301 single-inductor multi-output energy harvesting interface with double-conversion rejection technique and
302 buck-based dual-conversion mode. *IEEE Journal of Solid-State Circuits* 56, 961–971. doi:10.1109/
303 JSSC.2020.3025722
- 304 Kim, S., Vaidya, V., Schaef, C., Lines, A., Krishnamurthy, H., Weng, S., et al. (2018). A single-stage,
305 single-inductor, 6-input 9-output multi-modal energy harvesting power management ic for 100 μ w-
306 120mw battery-powered iot edge nodes. In *2018 IEEE Symposium on VLSI Circuits*. 195–196. doi:10.
307 1109/VLSIC.2018.8502301
- 308 Kuai, Q., Wan, Q., and Mok, P. K. T. (2019). A dual-frequency dual-input-dual-output interface for
309 thermoelectric energy harvesting and recycling with 82.9% efficiency. In *ESSCIRC 2019 - IEEE 45th*
310 *European Solid State Circuits Conference (ESSCIRC)*. 137–140. doi:10.1109/ESSCIRC.2019.8902863
- 311 Le, V. L., Yoo, T., Kim, J. E., Baek, K.-H., and Kim, T. T.-H. (2019). A 213.7- μ w gesture sensing
312 system-on-chip with self-adaptive motion detection and noise-tolerant outermost-edge-based feature
313 extraction in 65 nm. *IEEE Solid-State Circuits Letters* 2, 123–126. doi:10.1109/LSSC.2019.2935560
- 314 Lee, H.-H., Liu, C.-W., Takamiya, M., and Chen, P.-H. (2020a). Single-inductor dual-input dual-output
315 battery-pv hybrid system with 2-d adaptive on-time control for internet of things. *IEEE Transactions on*
316 *Circuits and Systems I: Regular Papers* 67, 1069–1078. doi:10.1109/TCSI.2019.2950330
- 317 Lee, S., Gandla, S., Naqi, M., Jung, U., Youn, H., Pyun, D., et al. (2020b). All-day mobile
318 healthcare monitoring system based on heterogeneous stretchable sensors for medical emergency.
319 *IEEE Transactions on Industrial Electronics* 67, 8808–8816. doi:10.1109/TIE.2019.2950842
- 320 Liu, C.-W., Lee, H.-H., Liao, P.-C., Chen, Y.-L., Chung, M.-J., and Chen, P.-H. (2018). Dual-source
321 energy-harvesting interface with cycle-by-cycle source tracking and adaptive peak-inductor-current
322 control. *IEEE Journal of Solid-State Circuits* 53, 2741–2750. doi:10.1109/JSSC.2018.2844358
- 323 Maeng, J., Park, I., Shim, M., Jeong, J., and Kim, C. (2021). A high-voltage dual-input buck converter
324 with bidirectional inductor current for triboelectric energy-harvesting applications. *IEEE Journal of*
325 *Solid-State Circuits* 56, 541–553. doi:10.1109/JSSC.2020.3012991

- 326 Martins, G. C. and Serdijn, W. A. (2021). An rf energy harvesting and power management unit operating
327 over -24 to +15 dbm input range. *IEEE Transactions on Circuits and Systems I: Regular Papers* 68,
328 1342–1353. doi:10.1109/TCSI.2020.3041175
- 329 Nagateja, T., Chen, S.-Q., Chu, L.-C., Chen, K.-H., Lin, Y.-H., Lin, S.-R., et al. (2019). A single-
330 inductor triple-output converter with an automatic detection of dc or ac energy harvesting source for
331 supplying 930.05mv/ma cross regulation to wearable electronics. In *2019 IEEE Asian Solid-State*
332 *Circuits Conference (A-SSCC)*. 49–52. doi:10.1109/A-SSCC47793.2019.9056895
- 333 Niu, S., Liu, Y., Zhou, Y. S., Wang, S., Lin, L., and Wang, Z. L. (2015). Optimization of triboelectric
334 nanogenerator charging systems for efficient energy harvesting and storage. *IEEE Transactions on*
335 *Electron Devices* 62, 641–647. doi:10.1109/TED.2014.2377728
- 336 Paidimarri, A. and Chandrakasan, A. P. (2017). A wide dynamic range buck converter with sub-nw
337 quiescent power. *IEEE Journal of Solid-State Circuits* 52, 3119–3131. doi:10.1109/JSSC.2017.2747217
- 338 Qian, Y., Lu, D., He, J., and Hong, Z. (2018). An on-chip transformer-based self-startup hybrid sidito
339 converter for thermoelectric energy harvesting. *IEEE Transactions on Circuits and Systems II: Express*
340 *Briefs* 65, 1673–1677. doi:10.1109/TCSII.2017.2773564
- 341 Qian, Y., Zhang, H., Chen, Y., Qin, Y., Lu, D., and Hong, Z. (2017). A sidido dc–dc converter with
342 dual-mode and programmable-capacitor-array mppt control for thermoelectric energy harvesting. *IEEE*
343 *Transactions on Circuits and Systems II: Express Briefs* 64, 952–956. doi:10.1109/TCSII.2016.2627551
- 344 Shim, M., Jeong, J., Maeng, J., Park, I., and Kim, C. (2019). Fully integrated low-power energy harvesting
345 system with simplified ripple correlation control for system-on-a-chip applications. *IEEE Transactions*
346 *on Power Electronics* 34, 4353–4361. doi:10.1109/TPEL.2018.2863390
- 347 Talkhoonchah, A. H., Yu, Y., Agarwal, A., Kuo, W. W.-T., Chen, K.-C., Wang, M., et al. (2021). A
348 biofuel-cell-based energy harvester with 86% peak efficiency and 0.25-v minimum input voltage using
349 source-adaptive mppt. *IEEE Journal of Solid-State Circuits* 56, 715–728. doi:10.1109/JSSC.2020.
350 3035491
- 351 Wang, C., Zhao, K., Li, Z., and Xiong, Q. (2020). Single-inductor dual-input triple-output buck–boost
352 converter with clockless shortest power path control strategy for iot nodes. *IEEE Transactions on Power*
353 *Electronics* 35, 2044–2052. doi:10.1109/TPEL.2019.2919945
- 354 Wang, Y.-H., Huang, Y.-W., Huang, P.-C., Chen, H.-J., and Kuo, T.-H. (2016). A single-inductor dual-path
355 three-switch converter with energy-recycling technique for light energy harvesting. *IEEE Journal of*
356 *Solid-State Circuits* 51, 2716–2728. doi:10.1109/JSSC.2016.2598222
- 357 Yang, G., Pang, G., Pang, Z., Gu, Y., Mäntysalo, M., and Yang, H. (2019). Non-invasive flexible and
358 stretchable wearable sensors with nano-based enhancement for chronic disease care. *IEEE Reviews in*
359 *Biomedical Engineering* 12, 34–71. doi:10.1109/RBME.2018.2887301
- 360 Zeng, Z., Estrada-López, J. J., Abouzied, M. A., and Sánchez-Sinencio, E. (2020). A reconfigurable
361 rectifier with optimal loading point determination for rf energy harvesting from -22 dbm to -2 dbm. *IEEE*
362 *Transactions on Circuits and Systems II: Express Briefs* 67, 87–91. doi:10.1109/TCSII.2019.2899338